



**HAL**  
open science

## Physical model for membrane protrusions during spreading.

François Chamaraux, Olivier Ali, Sébastien Keller, Franz Bruckert, Bertrand Fourcade

► **To cite this version:**

François Chamaraux, Olivier Ali, Sébastien Keller, Franz Bruckert, Bertrand Fourcade. Physical model for membrane protrusions during spreading.. *Physical Biology*, 2008, 5 (3), pp.36009. 10.1088/1478-3975/5/3/036009 . inserm-00347311

**HAL Id: inserm-00347311**

**<https://inserm.hal.science/inserm-00347311>**

Submitted on 15 Dec 2008

**HAL** is a multi-disciplinary open access archive for the deposit and dissemination of scientific research documents, whether they are published or not. The documents may come from teaching and research institutions in France or abroad, or from public or private research centers.

L'archive ouverte pluridisciplinaire **HAL**, est destinée au dépôt et à la diffusion de documents scientifiques de niveau recherche, publiés ou non, émanant des établissements d'enseignement et de recherche français ou étrangers, des laboratoires publics ou privés.

# Physical model for membrane protrusions during spreading

F. Chamaraux, O. Ali and B. Fourcade\*

*Université Joseph Fourier,  
Structure et Propriétés des Architectures Moléculaires,  
UMR 5819 CNRS, CEA-Grenoble,  
17 rue des Martyrs, 38054 Grenoble Cedex 9, France*  
and

*Inserm U823; Institut Albert Bonniot  
Centre de Recherche INSERM/ UJF U823-Equipe DYSAD  
Site Santé, La Tronche  
BP170 38042 Grenoble Cedex 9*

S. Keller, F. Bruckert

*École Nationale Supérieure de Physique de Grenoble,  
LMGP et Laboratoire de Biochimie et Biophysique des Systèmes Intégrés,  
UMR 5092 CNRS CEA-Grenoble, Département Réponse et Dynamique Cellulaires,  
17 avenue des Martyrs, 38054 Grenoble Cedex 09, France*

During cell spreading onto a substrate, the kinetics of the contact area is an observable quantity. This paper is concerned with a physical approach to model this process in the case of ameoboid motility where the membrane detaches itself from the underlying cytoskeleton at the leading edge. The physical model we propose is based on previous reports which point out that membrane tension regulates cell spreading. Using a phenomenological feedback loop to mimic stress dependent biochemistry, we show that the actin polymerisation rate can be coupled to the stress which builds up at the margin of the contact area between the cell and the substrate. In the limit of small variation of membrane tension, we show that the actin polymerisation rate can be written in closed form. Our analysis defines characteristic lengths which depend on elastic properties of the membrane-cytoskeleton complex, such as the membrane-cytoskeleton interaction, and on molecular parameters, such as the rate of actin polymerisation. We discuss our model in the case of axi-symmetric and non axi-symmetric spreading and we compute the characteristic time scales as a function of fundamental elastic constants such as the strength of membrane-cytoskeleton adherence.

PACS numbers: 87.17.Jj;87.16.Qp;87.15La

## Introduction

Cell motility is defined as the self-organized movement of living cells under the action of external stimuli[4]. Cells respond to mechanical perturbations and to chemo-attractant concentration variations, and this response drives slow differentiation and proliferation[33, 53, 62]. Using micro-contact patterning with sub-micrometer patterning, recent reports have shown that cell adhesion and cell motility can be studied at the individual cell level[12, 15, 64]. Because the substrates can be made transparent to optical microscopy, the observable quantity is the area of contact between the cell and the substrate. Red blood cells[10, 23], epithelial cells[61], fibroblasts[13, 18], neutrophils or monocytes[46] all spread but with different characteristic time scales and with different geometries for the contact line. The mechanisms involved in cell motility depend on the cellular type. Cells with focal adhesion and stress fibers have small migrating speed of the order of  $100 \text{ nm.s}^{-1}$ [57]. Ameobian cells with podosome-like adhesion[32] show, however, a higher speed of the order of a few microns per second. For these cellular models, such as *Dictyostelium discoideum* cells, hereafter referred as *D.d.* cells, the spreading characteristic time scale is of the order of the minute. It has been shown in [67] that *D.d.* amoeboid movement involve membrane protrusions initially free of F-actin cortical layer. These protrusions where the membrane is locally detached from the underlying cytoskeleton form away from the substratum [7, 9] and are followed by a gradual increase of F-actin cortical layer[67]. Motivated by these experimental findings, the physical model we consider assumes that actin polymerization at the margin of the contact area is associated with a local softening of the membrane cytoskeleton complex[6]. In this framework, we compute the kinetic of the increase of the contact area as a function of time.

---

\*Electronic address: Bertrand.Fourcade@ujf-grenoble.fr

Modern biological tools have considerably increased the molecular knowledge of the cytoskeleton organization and its relationship to cell motility and cell shape remodelling. In particular, the so-called dentritic nucleation model[48] has successfully explained the treadmilling of F-actin which polymerizes at the barbed ends. At the molecular level, it is known that actin remodelling involves phosphoinositide molecules, kinases and phosphatases as well as as small GTPase molecules[42, 47, 48, 52]. Although essential, the knowledge of the different proteins involved in the actin reorganization is not enough to understand macroscopic observables. Biochemical signals are mutually coordinated at large scale with mechanical stresses[40] and observations are made at a scale well above the molecular size of a typical protein. Different hypotheses have been proposed to explain actin-driven protrusions at larger scales both for *in vivo*[21, 28, 37–39, 60] and for purified *in vitro* systems (see Ref.[49] and [36] for a review), and it is likely that different cellular types use different mechanisms. As an example of stress-dependent signaling, we mention that Ref. [16, 20, 27, 41] have already pointed out the role of  $\text{Ca}^{2+}$  signalling through stretched or G-protein-activated  $\text{Ca}^{2+}$  channels for motility assays.

The physical model we consider in this paper describes the kinetics of growth of the contact area between a cell and the substrate. Our model is based on a few microscopic constants which characterize, for example, the adherence of the membrane to the cytoskeleton and the rigidity of the cell margin (see ref.[6] for a short account of the present work). Our analysis defines new characteristic length scales which may help to make the analysis of the rate of spreading more systematic. We hypothesize :

- that passive to active cooperative events are triggered by the contact between the cell and the substrate[5, 45, 63] ;
- that cell spreading is controlled by the adherence of the membrane to the cytoskeleton[51, 55? ]
- that actin polymerisation and depolymerisation rates are stress sensitive through the stress which builds up at the margin of the contact area when the cell spreads on the substrate.

The main result of this paper is that the characteristic curve of spreading has a linear regime as a function of time with a slope determined by these constants. In the next paragraph, we detail the experimental observations for *D.d.* cells which motivate the hypotheses of the physical model.

Our spreading model can be represented as a "pastry roll" which, when rolling, forces the rest of the cell to be in contact with the substrate. The rotation of the roll is due to actin polymerization in the adhesive belt. We make the hypothesis that this polymerisation is more stimulated because of the stress which builds up at the margin the contact area and we model this stress as a bending and a stretching energy for an imaginary line which symbolizes the complex formed by the membrane and the actin cortex. Although the exact link between actin polymerization and the contact with the substrate is not yet completely understood, experimental observations make this hypothese plausible. For example, there is a 10-fold increase at short times of the adhesive strength between the cell and the substrate after contact[19]. On the molecular side, talin which is a major link between the integrin and the cytoskeleton is recruited at the early stage of contact (1 s) under the control of the phosphoinositide  $\text{Pip}_2$  also involved in actin polymerization[34]. Third, the early steps of cell adhesion involve non-trivial time dependent membrane undulations and egress of bulky molecules[45]. Fourth, adhesive structures such as podosomes are found in motile cells and they display a very active actin turnover[8].

This active model differs from the viscous-elastic model proposed by Cuvelier et al. [11] which assumes that the kinetics of spreading is dominated at short time by the trade-off of a viscous component, which gives a characteristic time, and an elastic term. In this picture, spreading is seen as a passive phenomenon at short time. However, references [29, 30] report experimental observations which motivate the hypothesis made in this paper that spreading is an active phenomena. First, spreading of *D.d.* cell is highly anisotropic and is set by a polarization gradient set by some specific kinases, namely the PI3K family[52]. Second, spreading involves a well-coordinated movement of the contact line which shows protrusions with positive velocity parallel to the substrate, and retraction zones, with negative velocity[68]. Ref.[16] has shown that the movement of these zones is well coordinated even at short time. Third, cells can spread using more than one pseudopod at a time. This poses the question of what limits the extension of a pseudopod. In this work, we assume that a biochemical feedback loop triggered by the surface tension imposes a limit for the protrusion. In this paper, we do not consider the problem of what determines this quasi-periodic activity. Our problem is to know what can we learn from the shape of the spreading curve and we concentrate on one characteristic protrusion event.

This paper is organized as follows. The first section summarizes the hypotheses of the physical model. First, we present the axi-symmetric problem of spreading and we define characteristic length scales to describe the mechanical stresses in the adhesive belt. We introduce the shape problem to compute the speed parallel to the substrate as a function of the polymerisation rate constant. The model is based on the hypothesis that the extreme margin of the contact area can be modelled as a free membrane pushed towards the substrate as the contact area increases. The kinetic problem is solved in the axi-symmetric geometry and the rate of spreading is determined as a function

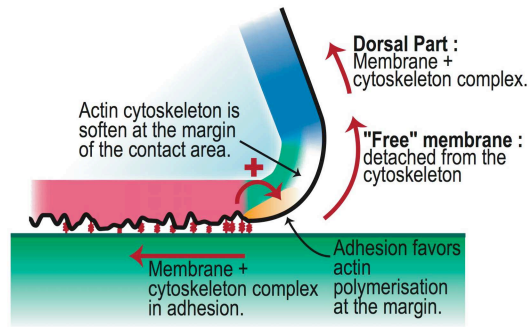


FIG. 1: Artist's cartoon of the cell border. The membrane and the cytoskeleton form a complex in adhesion with the substrate in the contact zone. We assume that this complex is softened in the immediate vicinity of the contact area on a length scale  $s_{max}$  ( see Eq. (24)). This part corresponds to segment  $AB$  of Fig. 2 and is considered as an effective membrane of bending modulus  $\kappa_m$ . The membrane-cytoskeleton complex in the dorsal part is a reservoir for the membrane pulled out during spreading.

of microscopic constants (see Eq. (47)). This section models the chemical feedback loop which regulates the actin polymerisation rate as a function of the mechanical stress. In the limit of small variations for the membrane tension during spreading, we show that the rate of biochemical reactions which govern actin polymerisation can be considerably simplified. Linearizing around the point where the rate of polymerisation balances the rate of depolymerisation renders the problem tractable without detailed knowledge of the biochemical mechanisms. The next section considers the non-axisymmetric problem with a membrane protrusion model. To simplify our vocabulary we will coin the word protrusion for these membrane protrusions, since they initially (i.e. before spreading) lack in F-actin cortex. This is in agreement with the definition made in [67] and the fundamental hypothesis made in this section is that protrusion occurs because of a local softening of the membrane-cytoskeleton interface at the margin of the contact area[3]. In this zone, the adherence between the membrane and the cytoskeleton is softened and the the membrane protrudes out. Because of actin polymerisation, the protrusion spreads on the substrate with a characteristic growth of the contact area.

Five appendices complete this work. The first defines an effective rate of actin polymerization in the adhesive belt. The second deals with the effect of a viscous flow for the membrane cytoskeleton attachment. The third details the variational shape equation used to compute the effective membrane shape near the contact line. The fourth contains geometrical calculations for the membrane protrusions. Finally, the fifth shows using a peeling model that the junction protrusion-cell is stressed during spreading.

## I. THE MODEL

From the geometrical point of view, we represent the shape of the membrane-cytoskeleton complex by a geometrical surface of height  $z(x, y)$  with respect to the substrate. In the most simple representation, the shape is an hemisphere with contact angle  $\theta$ . Actin polymerizes at the border of the contact area and the apparent contact angle increases during spreading. Fig. 1 and Fig. 2 give the schematic representation of the model which is summarized as follows :

1. Actin polymerisation takes place preferentially at the border of the contact area between the cell and the substrate. Thus, we assume that the contact between the cell and the substrate sends a molecular signal which increases the rate of filamentous actin polymerisation in the vicinity of the contact line. We will demonstrate that bending and stretching energy terms determine the shape problem.
2. The model includes the adhesion strength between the cell and the substrate. We mimic the link between the cytoskeleton and the substrate using an elastic foundation with a spring stiffness  $k$  which connects the height  $z(x, y)$  to the substrate[69]. We will assume that the distribution of these bonds is step like : in the referential of the adhesive belt of Fig. 2, all bonds are connected for  $x < 0$  but they are disconnected for  $x > 0$ . Cell spreading takes place at mechanical equilibrium. Minimization of the mechanical potential energy fixes the forces which, in turn, determine the rates at which actin is remodelled. Energies and stresses are calculated in the framework of continuum elasticity theory which is valid at the sub-micron scale. We assume that the numerous species of

proteins at work for cytoskeleton remodelling determine the elastic constants but we do not address the question of the exact molecular links between the proteins and the elasticity.

3. The model takes into account the attachment of the membrane to the cytoskeleton. If spreading takes place at constant volume, the membrane is pulled out of a reservoir to increase the apparent area of the cell at optical scales. We assume a continuous adhesion energy with an effective elastic coefficient. To mimic membrane traffic[1]during spreading, a chemical potential can be included[59]. The softening of the attachment of the membrane to the cytoskeleton near the margin of the contact area is essential in our model. This point has already been addressed in[3].
4. The actin polymerisation and depolymerization rates are stress-dependent at the margin of the contact area. Since the stresses are concentrated in this zone, this part of the cell is very sensitive to mechanical stimuli and this is where actin remodelling takes place. In particular, we will assume the cytoskeleton remodelling depends on a chemical stimulus. As an example, we mention that biochemical studies have demonstrated the essential role of external calcium in cell shape remodelling and adhesion. Since calcium fluxes control the concentration of calcium inside the cell[41], this suggests to take into account the activation of  $\text{Ca}^{2+}$  ionic channels [16]. Thus, the model assumes the following feedback loop : Channel activation  $\rightarrow$  Increase of  $[\text{Ca}^{2+}]$  concentration  $\rightarrow$  Cytoskeleton remodelling  $\rightarrow$  Spreading  $\rightarrow$  Adaptation of the stress at the margin of the contact zone. Other schemes are possible. For example, integrin like proteins occupancy can lead to the recruitment of molecular scaffold or adaptator proteins which in turn activate actin polymerisation and cytoskeleton remodelling[5]. The main point of this work is to show that the variations of tension are small during spreading. The presence of a small parameter from the physical point of view is crucial, since it allows to solve the kinetic problem by linearizing the rate equation for small surface tension variations.

Point 1 is standard in contact signalling. The contact between the cell and the substrate is receptor dependent which becomes, or which activates, an enzyme and catalyses the actin polymerization machinery. To compute the speed at which the cell spreads on the surface, we assume that the polymerization rate is normal to the cell membrane. The equation for the speed normal to the interface is the sum of an outward flux of polymerized actin minus an inward flux (point 4). Anticipating what follows, we write at point  $A$  of Fig. 2

$$V_{\perp}(\tau) = V_{+}[\tau] - V_{-}[\tau] \quad (1)$$

where  $\tau$  is the shear stress at the border of the contact zone (see later). At the early stages of spreading,  $V_{+} > V_{-}$ . Spreading stops when the stress  $\tau$  reaches  $\tau_{max}$  where  $V_{+}(\tau_{max}) = V_{-}(\tau_{max})$ . The exact functional form of  $V_{+,-}$  is very complex but we do not need to know it in details if we assume that the variations of the membrane tension are small during spreading. In this case, we approximate Eq. (1) by its linear variation around  $\tau_{max}$ .

Thus, we write

$$V_{\perp}(\tau) = V_{+}[\tau] - V_{-}[\tau] \approx \frac{dV^*}{d\tau} (\tau - \tau_{max}) \quad (2)$$

At the early stages of spreading,  $\tau$  is small, but it increases with the macroscopic angle of contact  $\theta$ . Spreading stops when the stress  $\tau$  is equal to  $\tau_{max}$ . Linearizing Eq. (2) introduces the phenomenological constant  $dV^*/d\tau$  which contains all the molecular biochemistry necessary to polymerize actin.

To compute the speed  $V_{\parallel}$  parallel to the substrate as a function of the speed  $V_{\perp}$  normal to the line  $z(x)$ , we consider the angle  $\psi$  between the tangent and the substrate. Since for  $\theta$  fixed the profile must be stationary, differential calculus [43] gives the functional form for  $V_{\perp}(x)$  (see Fig. 3)

$$V_{\perp}(x) = V_{\parallel}(\theta) \sin \psi(x, \theta) \quad (3)$$

which holds for any point of the line  $z(x)$  which represents the deformations of the adhesive belt.

Eq. (3) can now be inverted to yield at point  $A$  where  $x = 0$

$$V_{\parallel}(\theta) \approx \frac{V_{\perp}(\theta)}{\sin \psi_0(\theta)} \quad (4)$$

where  $V_{\perp}(\theta)$  can be replaced by the linear approximation Eq. (2). The reason for using point  $A$  to compute the velocity parallel to the substrate is that point  $A$  is the point where the stress of the adhesive bridges between the cytoskeleton and the substrate is maximum. Under the hypothesis made in Appendix A that  $d\psi/dt \simeq -k_{on}^0 \psi$ , or equivalently that  $V_{\perp}$  is proportional to the curvature, taking any point in the vicinity of  $A$  will give the same result.

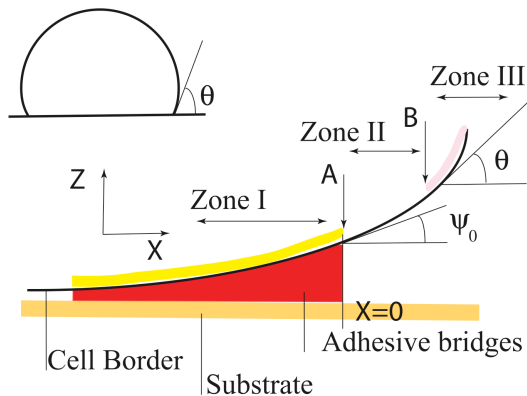


FIG. 2: Schematic view of a *D.d.* cell spreading on a substrate. When spreading is uniform along the contact line, the cell is represented as a hemisphere with contact angle  $\theta$  (top figure). The bottom figure illustrates the margin of the contact area where the cell leaves the substrate (adhesive belt). The grey part represents the adhesive matrix which connects the cytoskeleton to the substrate. The deformation energy stored in the adhesive belt is the sum of a curvature energy and of a stretching energy which are studied in this paper using a line  $z(x)$ . At the border of the contact zone, *i.e.* point A, the shape makes an angle  $\psi_0$  with the substrate. At point B, the shape matches the dorsal part of the top figure with a macroscopic contact angle  $\theta$ . Between points A and B, the cell is described by an effective free membrane.

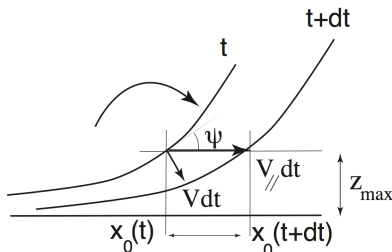


FIG. 3: Schematic view of the border of the contact area at two successive times. The cell adheres to the substrate via adhesive bridges which are connected to the substrate when the height  $z(x)$  is smaller than a cut-off  $z_{max}$ . By definition,  $z_{max}$  fixes the coordinate  $x_0(t)$  of the contact zone. We make the hypothesis that adhesion activates actin polymerisation at the margin of the contact area and induces an effective moment (schematized by the arrow, see Appendix A). When actin polymerizes, it pushes the membrane towards the substrate and the arrow symbolises the active moment defined in Appendix A. Between time  $t$  and  $t + dt$ , the border of the contact zone moves from  $x_0(t)$  to  $x_0(t + dt)$ . Assuming a layer by layer growth for actin remodelling, the growth takes place normal to the shape profile. Geometry gives the relationship (3) between the speed normal to the shape profile and the speed  $V_{\parallel}$  parallel to the substrate. When the tangent makes a small angle  $\psi$  with the substrate, we have  $V_{\parallel} \gg V$ .

Since  $\tau(\theta)$  depends on  $\theta$ ,  $V_{\perp}(\theta)$  depends on  $\theta$ . Eq.(4) with Eq. (2) is used in this paper to compute the area of contact as follows. Since for a circular area of contact of radius  $r(\theta)$ , we have  $V_{\parallel} = dr/dt$ , Eq. (4) is a differential equation for the kinetics of the area of contact. Eq. (4) shows also that the measurable rate of polymerization parallel to the substrate can be much larger than the physical polymerization rate perpendicular to line  $z(x)$ .

The next step is to determine the angle  $\psi(\theta)$  given by the balance of the mechanical forces. This is point 2. As it is the case for *D.d.*, we assume in what follows that the actin network forms a sheet of approximate thickness  $h_a \approx 0.5\mu\text{m}$  with different elastic properties. In parts I and III of Fig. 2, the membrane is in adherence with the cytoskeleton via a set of anchor proteins and it can invaginate within the cytoskeleton itself. According to this figure,

we divide the margin of the contact area into three zones with different elastic constants :

- The contact zone we call zone I extends to the point  $A$  where the first adhesive bridge connects the membrane-cytoskeleton complex to the substrate. Previous reports have concentrated on this adhesive belt and they have shown that the typical width of the zone where the adhesive bridges are stretched is of the order  $\xi \approx 0.1\mu\text{m}$ [17]. In physical terms, this zone is an elastic foundation with an elastic modulus  $k$  and an effective bending rigidity  $\kappa_a \approx \text{few hundred k}_\text{B}\text{T}$ [54].
- In zone II, between points A and B, the interface is soft. This is the zone where actin remodeling is very active and we consider this zone as an effective membrane with a bending rigidity  $\kappa_m \approx 50\text{k}_\text{B}\text{T} \ll \kappa_a$  and a surface tension  $\sigma$ . The maximum distance  $z_{max}$  under which the adhesives bridges are connected to the substrate scales with  $\xi$  as[17]

$$z_{max} = \frac{\xi^2}{2R_A} \quad (5)$$

where  $R_A$  is the radius of curvature of the osculating circle at the contact line (at point A).

- Finally, in zone III, the membrane and the cytoskeleton form a complex. This part gives the reservoir from which the membrane can be pulled out when the cell spreads on the surface.

Pulling out the membrane from this reservoir implies that the surface tension  $\sigma$  in part II increases by an amount proportional to the relative increase of area :

$$d\sigma = C \frac{dA}{A} + \eta \frac{d}{dt} \left[ \frac{dA}{A} \right] \quad (6)$$

where  $A$  is the total area (see point 3). The first term is the elastic contribution to the stress. By definition,  $C$  is a constant which measures the strength of the attachment of the membrane with an order of magnitude of 50 pN.nM. The second term is proportional to the rate at which the relative area is pulled out and it simulates the effect that the relative increase of area pulled by a sudden increase of tension  $\Delta\sigma$  is equal to  $1/C\Delta\sigma$  only after a time  $\eta/C$ . It characterizes the long time behavior of the viscoelastic response and it simulates membrane flow[2]. We show in Appendix B that this term does not affect the short time behavior for spreading since the short time is independent of the increase of tension.

Finally, point 4 is an assumption based on biochemical studies. Experiments on motility have shown that  $\text{Ca}^{2+}$  ionic channels activated by G-protein-coupled receptors play an important role in cell motility. These receptors can be activated upon application of forces in the pN range[22]. Thus, the concentration of stress at the margin of the contact area implies that the actin turnover is amplified at the rim and that the rates of polymerisation and depolymerisation depend on  $\tau_{x,z}$  ( the shear stress  $\tau_{x,z}(x)$  is proportional to the surface tension  $\sigma$  and is defined in section IV).

The rest of the calculation follows this framework. We compute the speed at which the membrane spreads with formula (3) calculated at point A at the border of the adhesive belt. When the contact area increases, the angle  $\psi$  increases, since tension is build in part II. In turn, increasing the tension increases the shear stress and limits the actin polymerisation rate.

## II. AXI-SYMMETRIC SPREADING

This section is concerned with the calculation of the surface tension  $\sigma(\theta)$  which controls the rate at which actin is polymerized. For simplicity, we will ignore the viscous component in Eq.(6), i.e.  $\eta = 0$ . We schematize the shape of the cell as an hemisphere. The dorsal part is a spherical cap of radius  $R(\theta)$  with a macroscopic contact angle  $\theta$ . When the cell starts spreading  $R = R_i$ . It increases with time as the contact radius  $r(\theta)$  does. The area of contact is  $A = \pi r^2(\theta)$  and between time  $t$  and  $t + dt$  the radius  $r$  increases from  $r$  to  $r + dr$  (see Fig. 2).

Geometry gives the relationship between  $R_s(\theta)$  and  $\theta$

$$R_s(\theta) = 4^{1/3} \frac{R_i}{[(1 + \cos \theta)^2 (2 - \cos \theta)]^{1/3}} \quad (7)$$

so that the contact radius is

$$r(\theta) = R_s(\theta) \sin \theta \quad (8)$$

TABLE I: List of symbols with their order of magnitude

Parameter	Notation	Value
Size	$R_i$	5 $\mu\text{m}$
Characteristic tension for channel opening[22, 58]	$\sigma_{1/2}$	5 pN.nm <sup>-1</sup>
Polymerization speed at zero stress[4]	$V_+^0$	100nm.s <sup>-1</sup>
Parameter $dV^*/d\sigma \approx -V_+^0/\sigma_{1/2}$		-20 nm <sup>2</sup> .pN <sup>-1</sup> .s
Width of the adhesive belt	$\xi$	0.1 $\mu\text{m}$
Actin rigidity characteristic length	$\lambda_a^{-1}$	$\approx \xi$
Screening length of the adhesive matrix	$\lambda_m^{-1}$	$\approx \xi$
Membrane correlation length	$\lambda^{-1}$	> 10 nm
Membrane-cytoskeleton attachment[58]	C	50 pN.nm <sup>-1</sup>
contact angle[56]	$\theta_{max}$	1 rad.

For what follows, it will be useful to consider other geometries. For an hemi-cylinder of radius  $R_A(\theta)$

$$R_A(\theta) = \pi^{1/2} R_i \left[ \frac{1}{\pi - \theta + 0.5 \sin 2\theta} \right]^{1/2} \quad (9)$$

with an equivalent formula as before for the contact radius.

In order to compute the surface tension  $\sigma$ , we define  $\mathcal{A}_d$  as the area of the dorsal part.  $\mathcal{A}_d$  is also a function of  $\theta$  as

$$\mathcal{A}_d(\theta) = 2\pi R_s^2(\theta) (1 + \cos \theta) \quad (10)$$

When the cell spreads by an infinitesimal amount,  $\theta \rightarrow \theta + d\theta$ , the contact area increases by  $d\mathcal{A}_r(\theta) = 2\pi r dr$  and membrane has been taken out of the reservoir by an amount

$$\frac{d\mathcal{A}}{\mathcal{A}} = \frac{1}{\mathcal{A}(\theta)} [\mathcal{A}_d(\theta + d\theta) + d\mathcal{A}_r(\theta) - \mathcal{A}_d(\theta)] \quad (11)$$

where  $d\mathcal{A}_r$  is the small piece in contact with the substrate when  $\theta$  increases. Using Eq. (6) with  $\eta = 0$ , we compute the tension  $\sigma(\theta)$  as (in circular geometry)

$$\sigma(\theta) = \sigma_0 + C \ln \left[ \frac{\mathcal{A}_d(\theta)}{\mathcal{A}_d(\theta = 0)} \right] + C \int_0^\theta du \frac{2\pi r(u) dr}{\mathcal{A}_d(u) du} \quad (12)$$

When  $\theta$  is small, it is enough to approximate  $\sigma(\theta)$  by the leading terms

$$\sigma(\theta) = \sigma_0 + \frac{1}{16} C \theta^4 + \dots \text{circular geometry} \quad (13)$$

$$\sigma(\theta) = \sigma_0 + 0.053(\dots) C \theta^3 + \dots \text{cylindrical geometry} \quad (14)$$

Eqs. (13) and (14) are still valid when  $\theta$  is large. The reason for this is that the divergence of  $\sigma(\theta)$  is only logarithmic when  $\theta$  approaches  $\pi$

$$\sigma(\theta) \propto C \ln(\pi - \theta), \theta \rightarrow \pi \quad (15)$$

where the proportionality constant depends on the geometry.

### III. CELL CONTOUR AT MECHANICAL EQUILIBRIUM

#### A. Soft zone

Let us consider the zone II of Fig. (2). In this zone, the cell cortex is soft with an effective bending rigidity  $\kappa_m$  and a tension  $\sigma(\theta)$ . The surface tension  $\sigma$  is taken as constant, since there is no tangential force to equilibrate surface

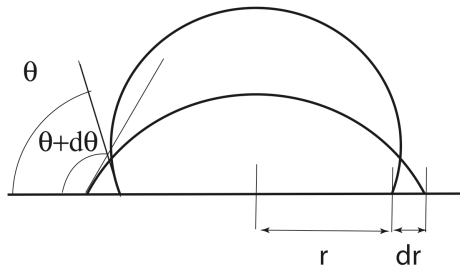


FIG. 4: Side view of the cell body when the macroscopic contact angle  $\theta$  varies. As explained in the text, to increase the contact area  $\mathcal{A}(t) = \pi r^2(t)$ , membrane is taken out of a buffer which supplies the part between  $r$  and  $r + dr$  and the increase of the dorsal part. The figure applies to the spherical geometry where the cell is viewed as an axi-symmetric hemisphere or to the cylindrical geometry where the axis is perpendicular to the figure. In the spherical geometry, the radius of the hemisphere is noted  $R_s(\theta)$ .

tension gradient. The profile can be parametrized using the angle  $\phi$  between the tangent and the direction fixed by the macroscopic angle  $\theta$ . If  $\psi$  is the angle between the tangent and the substrate, geometry gives

$$\psi + \phi = \theta \quad (16)$$

To find  $\psi(s)$ , we minimize the Helfrich-Caham potential at fixed macroscopic angle  $\theta$ . Let  $\mathbf{u}_\theta$  be the unit vector in the direction  $\theta$  and  $\mathbf{t}(s) = dx/ds\mathbf{u}_x + dy/ds\mathbf{u}_y$  be the tangent along the arc (between  $A$  and  $B$  in Fig. 2). The total potential which includes the work done by the tension in the direction  $\mathbf{u}_\theta$  is

$$F = \frac{1}{2}\kappa_m \int_A^B ds \left( \frac{d\psi}{ds} \right)^2 - \sigma \int_A^B ds \mathbf{u}_\theta \cdot \mathbf{t}(s) \quad (17)$$

with  $\mathbf{u}_\theta \cdot \mathbf{t}(s) = \cos \phi(s)$ . Taking the scalar product is necessary, since the work done by the tension is proportional to the displacement of  $B$  in the direction  $\mathbf{u}_\theta$  with

$$\sigma \mathbf{u}_\theta \cdot \int_A^B ds \mathbf{t}(s) = \sigma \mathbf{u}_\theta \cdot \mathbf{AB} \quad (18)$$

To solve the variational problem, we use  $\phi(s)$  as the independent variable (see appendix C). The Euler equation reads as

$$\kappa_m \frac{d^2 \phi}{ds^2} - \sigma(\theta) \sin \phi(s) = 0 \quad (19)$$

where the solution satisfies the boundary conditions :

1. On the one side, the shape matches tangentially to the contact zone. Both the force in the direction normal to the substrate,  $\kappa_a y'''(x = 0-) = \kappa_m y'''(x = 0+)$ , and the bending moment,  $\kappa_a y''(x = 0-) = \kappa_m y''(x = 0+)$  equilibrate at point A. These conditions assume small bending and they are only valid if the radius of curvature  $R_A$  of the rim is large enough for the force normal to the substrate to be approximated by the third derivative. We will see that this condition is fulfilled in the limit  $R_A \lambda_a \gg 1$ , where  $\lambda_a^{-1}$  is an elastic characteristic length scale (to be defined in Eq. (27)). Explicit expressions for second and third derivatives can be found by multiplying Eq. (19) by  $d\phi/ds$ .

2. On the other side, the shape matches tangentially the contact sphere at point B where the membrane adheres to the cytoskeleton again. Thus we have  $\phi = 0$  and  $d\phi/ds = 1/R(\theta)$ . These conditions assume that the membrane is pulled out of from the cytoskeleton at angle  $\theta$ . To define an angle of contact  $\theta$ , we must demonstrate that  $s_{max}$  is small compared to the radius  $R(\theta)$ .

To see this, we integrate Eq. (19) with  $\lambda = \sqrt{\sigma(\theta)}/\kappa$ . We get :

$$\frac{d\phi}{ds} = \lambda(\theta) [2 + \lambda^{-2}R^2(\theta) - 2\cos\phi]^{1/2} \quad (20)$$

with  $d\phi/ds = 1/R(\theta)$  when  $\phi = 0$  at  $B$ . Thus

$$s_{max} = \int_{\phi=0}^{\phi=\phi_0} d\phi \left[ \frac{ds}{d\phi} \right] \quad (21)$$

$$= \lambda^{-1}(\theta) \int_{\phi=0}^{\phi=\phi_0} d\phi \left[ \frac{1}{2 + \lambda^{-2}R^2(\theta) - 2\cos\phi} \right]^{1/2} \quad (22)$$

$$(23)$$

where  $\phi_0$  is the angle between the tangent at point A. In general,  $0 \leq \phi \leq \theta$ . This equation shows that the membrane correlation length  $\lambda^{-1}(\theta)$  sets the length  $s_{max}$ . This integral is only logarithmic divergent when  $\theta$  approaches  $\pi$  as

$$s_{max} \approx \left[ -\frac{\kappa_m}{C} \ln(\pi - \theta) \right]^{1/2} \quad (24)$$

within a numerical factor which depends on the geometry. Thus  $s_{max}$  is of the order of the length  $\lambda^{-1}(\theta)$  and it remains small as long as  $\theta$  does not approach  $\pi$ . As a result we can define a contact angle independent of the cell shape.

## B. Contact zone

In zone I, the cell is connected to the substrate via a complex set of proteins we call adhesive bridges. The simplest approach assumes a uniform density of connectors  $n_b$  with spring constant  $k$  between the membrane - cytoskeleton complex and the substrate. The equilibrium height profile  $z(x)$  obeys the Euler equation

$$\kappa_a \frac{d^4 z}{dx^4} - \sigma \frac{d^2 z}{dx^2} + n_b k z(x) = 0 \quad (25)$$

where  $\sigma$  is the in-plane tension and  $\kappa_a$  the bending rigidity. In continuum mechanics,  $\sigma$  is proportional to a force applied to the membrane-cytoskeleton complex parallel to the substrate before bending. We take  $\sigma = 0$  since the adhesive belt is a zone which is dominated by curvature and, to leading order, surface tension gradients which scale with maximum value of  $z(x)$ , i.e.  $z_{max}$ , appear only in the tangential force balance equation (see section IV). The characteristic equation of Eq. (25) has the solutions :

$$\lambda = \pm \frac{1}{\sqrt{2}} (1 \pm i) \lambda_a \quad (26)$$

with a new characteristic length

$$\lambda_a = \left( \frac{kn_b}{\kappa_a} \right)^{1/4} \quad (27)$$

where  $\lambda_a^{-1}$  is of the same order of magnitude than the adhesive belt width  $\xi$ . Since the shape profile must match the substrate for  $x \rightarrow -\infty$ , we solve Eq. (25) as

$$z(x) = [\mathcal{A}(\theta) \sin(\lambda_a x) + \mathcal{B}(\theta) \cos(\lambda_a x)] \exp[\lambda_a x], x < 0 \quad (28)$$

where the two constants  $\mathcal{A}(\theta)$ ,  $\mathcal{B}(\theta)$  are determined by matching with the outer solution (see Eq. 19) where the membrane is free. The next section presents this calculation.

### C. Matching conditions

To derive the matching conditions at point A of Fig. 2, we make use of the fact that the mechanical constraints balance each other at  $x = 0$ . Equality of the tangent, of the normal forces (third derivative of the shape profile) and of the bending moments (second derivative of shape profile) leads to the system of equations [31, 35]

$$\lambda_a (\mathcal{A}(\theta) + \mathcal{B}(\theta)) = \psi_0(\theta) \quad (29)$$

$$2\lambda_a^3 (\mathcal{B}(\theta) - \mathcal{A}(\theta)) = \frac{\kappa_m}{\kappa_a} \lambda^2(\theta) \sin(\theta - \psi_0(\theta)) \quad (30)$$

$$2\lambda_a^2 \mathcal{A}(\theta) = \frac{\kappa_m}{\kappa_a R(\theta)} \left[ 1 + 4 \frac{\kappa_a^2}{\kappa_m^2} \lambda^2(\theta) R^2(\theta) \sin^2(\theta/2 - \psi_0(\theta)/2) \right]^{1/2} \quad (31)$$

To make analytical progress, we first assume the following two limit cases :

$$\frac{\kappa_a^2}{\kappa_m^2} \lambda(\theta) R(\theta) \gg 1 \text{ (Large protrusion)} \quad (32)$$

$$\lambda_a^{-1} \ll \lambda^{-1}(\theta) \text{ (Small tension)} \quad (33)$$

and we get simple results

$$\mathcal{A}(\theta) = \mathcal{B}(\theta) \quad (34)$$

$$2\lambda_a^2 \mathcal{A}(\theta) = 2\lambda(\theta) \sin(\theta/2) \text{ (Curvature at point A)} \quad (35)$$

$$\psi_0(\theta) = 2 \frac{\lambda(\theta)}{\lambda_a} \sin(\theta/2) \quad (36)$$

As a consequence, the angle  $\psi_0$  between the tangent and the substrate at the margin of the contact area increases with the contact angle  $\theta$ . Using the last two equations of (35) shows that the product of  $\psi$  by the radius of curvature  $R_A$  is constant on the scale  $1/\lambda_a$  of the adhesive belt :

$$\psi(\theta) R_A = \frac{1}{\lambda_a} \text{ ( independent of } \theta \text{)} \quad (37)$$

This property is used in Appendix A to show that Eq. (3) is equivalent to define the velocity  $V_\perp$  as proportional to the curvature along the meridian.

Because the constants  $\mathcal{A}(\theta)$  and  $\mathcal{B}(\theta)$  are known, the shape profile  $z(x)$  follows from Eq. (28). The total energy stored in the adhesive belt can now be calculated as :

$$\mathcal{E}_{\text{belt}} = 2\kappa_a \lambda_a^{-4} \lambda(\theta)^3 \sin^2(\theta/2) \quad (38)$$

where the respective contribution of the stretching and bending elastic term are equivalent. This formula shows that the increase of energy stored in the adhesive belt is quadratic with the macroscopic contact angle  $\theta$ .

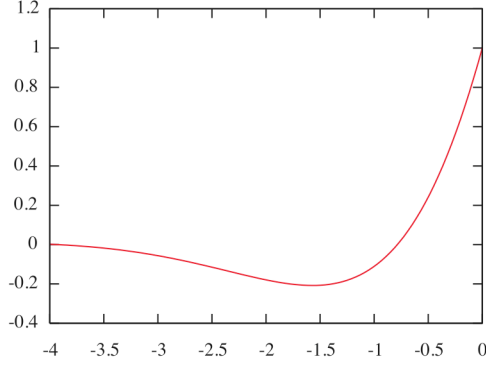
To conclude, we note that the matching conditions for the bending moment and the normal force at the border of the adhesive belt specify the height  $z(x=0)$ . We have :

$$z(x=0) = \frac{\lambda(\theta)}{\lambda_a^2} \sin \theta/2 \ll \lambda_a^{-1} \quad (39)$$

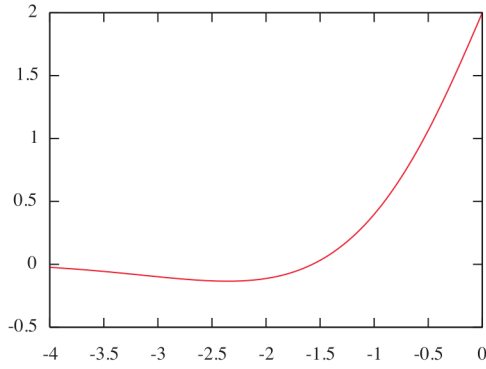
Eq. (28) demonstrates that the shape profile is a damped sinusoid with a scale  $\lambda_a^{-1}$  along the normal of the contact zone and parallel to the substrate (see Fig. 5). Thus our solution predicts that the adhesive zone is compressed at the margin of the contact area and that the distance between the cell and the substrate is larger in the core of the adhesive area than at the rim. The width of this compressed zone is set by the density of density  $n_b$  of adhesive bridges, and it is of the order of  $\lambda_a^{-1} \approx 0.1 \mu m$ . Thus experiments probing the strength of the adhesion in the contact zone should see a dark rim when the contact zone is imaged from below by reflection contrast microscopy.

### IV. TANGENTIAL FORCES

Eq. (25) is the equation for the mechanical forces in the direction normal to the substrate. In this section, we concentrate on the direction tangent to the substrate and we include surface tension gradients. To derive the condition



(a)



(b)

FIG. 5: Plot of the height profile  $\exp(\lambda_a x)(\cos(\lambda_a x) + \sin(\lambda_a x))$  as a function of  $\lambda_a x$ . By definition, the margin of the contact area ends at  $x = 0$ . This plot shows that the adhesive zone is first compressed at the rim of the contact area between the cell and the substrate. Near the frontier at  $x = 0$ , on a width which scales as  $\lambda_a^{-1}$ , the adhesive bridges are stretched. Thus, the force normal to the substrate changes sign in the adhesive belt whose frontier is at  $x = 0$ . Case (b) : Plot of the derivative of the shape profile as a function of  $\lambda_a x$ . Since  $V_{\perp} \propto \psi$  (see Eq. (3)) with  $\psi \approx dh/dx$ , the speed normal to the line can change sign.

for equilibrium, we include the typical distance  $h_a \approx 50$  n.m. between the cell and the substrate in the contact zone ( $x \rightarrow -\infty$ ). Let  $h_b \approx 100$  n.m. be the thickness of the actin layer in the contact zone (see Fig. IV).

The calculation of Ref.[35] illustrates this point. Let us consider a displacement  $u$  in the  $x$ -direction. The shear stress  $\tau_{x,z} = \mu_a u/h_a$  in the adhesive matrix equilibrates the tensile stress  $\sigma_{xx} = Edu/dx$  in the actin layer with

$$\frac{d\sigma_{xx}}{dx} = \frac{\tau_{xx}(x)}{h_b} \quad (40)$$

$E$  and  $\mu_a$  are the Young modulus of the actin layer and  $\mu_a$  is the shear stress elastic constant for the adhesive bridges. By definition of the tensile stress, we have  $\sigma = h_b \sigma_{xx}$  where  $\sigma$  is the surface tension. Solving these equations gives that the shear stress and the tensile stress  $\sigma_{xx}$  are screened on a characteristic distance

$$\tau_{xz}(x) = \begin{cases} \tau_{xz}(0) \exp[\lambda_m x] & \text{for } x \leq 0 \\ 0 & \text{for } x > 0 \end{cases} \quad (41)$$

with

$$\lambda_m = \left( \frac{\mu_a}{E h_b h_a} \right)^{1/2} \quad (42)$$

This exponential dependence explains the independence of the mechanical equilibrium in the adhesive belt of the contact area. Depending on the geometry, two cases are of interest (see Fig. IV).

1. When matching the actin layer with the membrane in done on the mid-plane of the actin layer at  $z(x)$ , we find :

$$\tau_{xz}(0) = \sigma \lambda_m \cos \theta \quad (43)$$

2. However, it is likely that the matching should be done at the lower layer  $z(x) - h_b/2$  where the flexion stress  $\sigma_{xx} = Ez''(0)h_b/2$  is maximum, since the actin cortex is always beneath the membrane. Thus we sum up the tensile stress and the flexural stress so that by Eq. (35)

$$\tau_{xz}(0) = E h_b \lambda(\theta) \sin \theta/2 + \sigma \lambda_m \cos \theta \quad (44)$$

Taking  $E \approx \mu_a$  gives  $\lambda_m^{-1} \approx$  a few tenth of nm. Thus, all characteristic length scales,  $\lambda_m$ ,  $\lambda_a$  and  $\xi$  are of the same order and we will take them as equal.

To study the influence of the elasticity of the substrate we add a third layer with shear rigidity  $\mu_s$  (see Fig. IV). Thus the composite layer adhesive matrix + substrate has an effective rigidity  $\mu_{eff}$  dominated by the rigidity of the substrate ( $\mu_{eff}^{-1} = \mu_{substrate}^{-1} + \mu_a^{-1}$  for two elastic springs in series) if the former is sufficiently soft. Going back to the definition (42) of the screening length, we see that the shear stress is less localized on soft substrates than they are on rigid ones. This result is consistent with the hypothesis that position and force dependent phosphorylation mechanisms for actin polymerisation may depend on the shear rigidity of the substrate.

## V. SPREADING WITH UNIFORM POLYMERIZATION ALONG THE CONTACT LINE

In the framework of our model, see Eq. (1), the rate of polymerization is fixed by the ratio  $V_+/V_-$  which is larger than one when actin polymerization is more enhanced in the adhesive belt. In the limit case, where the tension build in the membrane does not increase too much, we can linearize the rate of polymerization as in Eq. (2) so that

$$V_{\parallel} \approx \frac{dV^*}{d\sigma} \frac{\sigma(\theta) - \sigma_{max}}{\psi(\theta)} \quad (45)$$

with  $dV^*/d\sigma < 0$  and  $V_{\parallel}(\sigma(\theta_{max})) = 0$ . Since both  $\sigma(\theta)$  and  $\psi(\theta)$  are known functions of  $\theta$  (see Eqs. (12) and (36)), Eq. (45) is a differential equation for the kinetics of the contact growth as a function of time, since  $V_{\parallel}$  is proportional to  $d\theta/dt$ .

To integrate this equation, we use the angle  $\theta$  as a variable.

$$\frac{d}{dt} \left[ \frac{\theta^2}{\theta_{max}^2} \right] = -\frac{\alpha}{\theta_{max}^4} (\theta^4 - \theta_{max}^4) \quad (46)$$

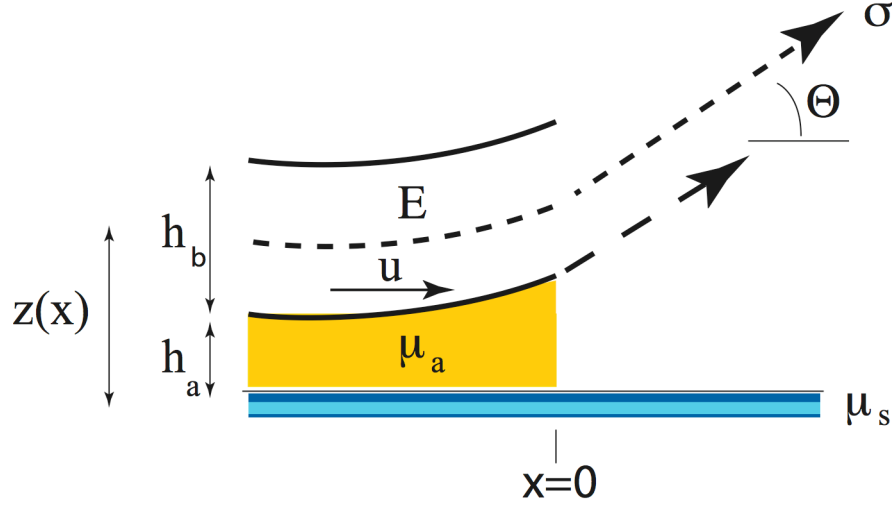


FIG. 6: Schematic view of the actin layer of thickness  $h$  and Young modulus  $E$ . This Figure concerns section IV. The adhesive bridges are represented as an elastic foundation of height  $h_a$  and shear rigidity  $\mu_a$ . The effect of flexible substrate can be studied by adding a third layer of shear rigidity  $\mu_s$ . The displacements  $u$  are tangent to the substrate. The two cases of section IV are schematized in this Figure. If the matching between the actin cortex and the membrane is done at  $x=0$  in the midlayer (see Eq. (43)) the tension is applied along the dashed line. If the matching is done in the lower layer (see Eq. (44)), this corresponds to a tension applied along the long-dashed line.

where the characteristic time  $\alpha^{-1}$  is given by

$$\alpha = -\frac{1}{R_i} \frac{\lambda_a}{\lambda_0} \frac{\sqrt{C}}{2} \frac{dV^*}{d\sigma} \sqrt{\sigma_{max} - \sigma_0} \quad (47)$$

with  $\lambda_0 = \sqrt{\sigma_0/\kappa_m}$ . Because  $\alpha$  depends on the square root of the relative increase of tension,  $\Delta\sigma/\sigma$ , this indicates that the rate of spreading is very sensitive to small variations of the tension at rest  $\sigma_0$ . Integrating now Eq. (46), we find that the growth of the contact area behaves as

$$\frac{\mathcal{A}_{\text{contact}}}{\mathcal{A}_{\text{max}}} = \tanh \alpha t \quad (48)$$

where the growth is linear at short time before it saturates on a characteristic time scale  $1/\alpha$ . The linear regime is only valid for large protrusions where  $\kappa_a/\kappa_m \lambda(\theta) R(\theta) \sin(\theta/2) \gg 1$ . This condition gives a crossover angle

$$\theta_{\text{crossover}} \approx \frac{1}{\lambda_0 R_i} \left[ \frac{\kappa_m}{\kappa_a} \right]^{1/2} \quad (49)$$

Since  $\kappa_m/\kappa_a \approx 0.1$ ,  $\theta_{\text{crossover}}$  is observable for small enough protrusions of the order of the micron. To get the area of contact as a function of time, we solve Eqs. (29) numerically. As shown in Fig. 7, the growth of the contact area is quadratic at short time and it crosses over to the linear regime predicted by (48) above.

Eq. (47) predicts that the kinetics of spreading depends on characteristic parameters which vary from cells to cells. Its order of magnitude can be estimated using Table I and the following reasoning. The derivative  $dV^*/d\sigma$  is of the order of  $V_+^0/\sigma_{1/2}$  where  $\sigma_{1/2}$  is the characteristic tension where half of the channels are open[22]. Using a maximum contact angle of  $\theta_{max} = 1$  rad and assuming a size of  $5 \mu\text{m}$  gives  $\alpha = 0.03 \text{ s}^{-1}$  which compares with experimental data (see the discussion section at the end of the paper).

We now turn to the cylindrical geometry where the cell spreads perpendicular to its axis. Calculations are similar as before. Using Eq. (14) for the variation of surface tension at small contact angle gives

$$\frac{d\theta^2}{dt} = \frac{2}{R_i} bC \frac{\lambda_a}{\lambda(\theta)} \left( -\frac{dV^*}{d\sigma} \right) (\theta_{max}^3 - \theta^3) \quad (50)$$

where  $b$  is a numerical constant (0.053...). In the cylinder case, the contact area is proportional to  $\theta$  and not to  $\theta^2$ , since

$$\mathcal{A}(t) \approx R_i \theta L \quad (51)$$

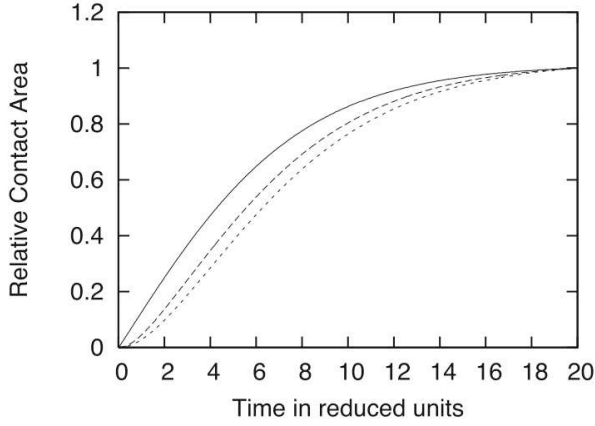


FIG. 7: Growth of the contact area with time for the axi-symmetric case. Curves are obtained by solving numerically the matching conditions (see Eqs. (29)). This Figure illustrates how the shape of the spreading curve depends on the ratio of the size of the protrusion to the characteristic length  $\lambda_0^{-1}$ . When the size of the protrusion  $R_i$  is small enough, the quadratic behavior at short time scale is clearly visible (see the definition of  $\theta_{\text{crossover}}$  defined in Eq. (49)). From the bottom curve to the top one,  $\kappa_m/\kappa_a R\lambda_0 = 1.6, 2.3, 50$ . Time is scaled by  $k_{\sigma n}^0 (= 1)R(\theta = 0)\lambda(\theta = 0)/\lambda_a$ .

where  $L$  is the width of the cylindrical protuberance. As before, we write the equation of the kinetics of the contact area

$$\frac{d}{dt} \left[ \frac{\mathcal{A}^2(t)}{\mathcal{A}_m^2} \right] = \alpha' \left( 1 - \left( \frac{\mathcal{A}(t)}{\mathcal{A}_m} \right)^3 \right) \quad (52)$$

where the time scale factor  $\alpha'$  is different from above

$$\alpha' \approx -0.28 \frac{dV^*}{d\sigma} \frac{C^{1/3} \sigma_0^{1/3} \lambda_a}{\lambda_0 R_i} (\sigma_{max}/\sigma_0 - 1)^{1/3} \text{ (cylinder)} \quad (53)$$

From Eq. (52), the contact area scales as  $\sqrt{t}$  instead of  $t$  at short time. The time scale factor is a non-integer power of  $\Delta\sigma/\sigma$  with a numerical estimate of  $10^{-3}$  which is smaller than before. This calculation illustrates how the geometry changes the spreading curve, but the cylindrical case is specific since the growth rate is independent of the width  $L$  of the protuberance.

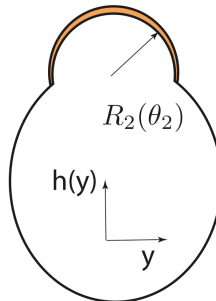


FIG. 8: Model for the non-axi-symmetric spreading case. A protrusion is schematically represented as an hemispherical cap of radius  $R_2(\theta_2)$  spreading out of a mother cell. We assume that the membrane-cytoskeleton complex is fully intact in the mother cell. The protrusion spreads on the substrate because actin polymerizes at the edge of the spherical cap.

## VI. NON AXI-SYMMETRIC SPREADING

From now on, we consider the non-axisymmetric spreading problem, and we assume that the membrane-cytoskeleton adhesion can be locally softened around the margin of the contact area. Fig. 9 schematizes the geometry we will consider henceforth. The membrane cytoskeleton-complex is intact around the cell border, but it is locally softened along the top arc of circle of the figure. This softening occurs because of a biochemical reaction which ruptures the linkage between the membrane and the cytoskeleton. When the membrane is free, it can be pushed outwards by osmotic pressure. It produces a hyaline spherical protrusion called a bleb in the biological literature. It is not the purpose of the model to characterize the process of bond rupture. We simply assume that the membrane is detached from the cytoskeleton between the two end points at a distance  $2d(\theta_2^0)$ .

This problem is geometrically equivalent to the one we have studied before and our variational calculation is based on the following hypotheses :

1. In order for the stress parallel to the substrate to be decoupled from the stress normal to the substrate we assume[31]:

$$R(\theta_2)\lambda_a \gg 1 \quad (54)$$

In the other limit, the force normal to the substrate depends on the radius of curvature in the plane of the substrate and the previous calculation does not apply.

2. The rate of polymerisation is constant along the contact line formed by the protrusion and the substrate. This constraint imposes that the contact line with the substrate is a circle. Thus, we cannot solve the mechanical force balance equations on the line of contact between the cell and the protrusion and we will only give asymptotic results using effective contact angle.

Let  $R_2$  be the radius and  $\theta_2$  the contact angle. Because of actin polymerisation, the protrusion spreads on the substrate with  $\theta_2(t)$  being a function of time  $t$  and  $\theta_1$  being constant. We work in the limit where of small protrusion,  $R_2(\theta_2) \ll R_1(\theta_1)$  with  $\theta_1$  is fixed. In this limit, the position of the contact line on the substrate is labelled by the height variable  $h(y)$ . During spreading on the substrate, we assume that the contact line describes a family of circular arcs labelled by the angle  $\beta$  between the tangent and the  $h = 0$  axis (see Fig. 9 and Appendix D)

Two cases are of interest :

1. The protrusion is a spherical cap and the membrane is taken from the protrusion itself without membrane traffic between the cell and the protrusion.
2. The protrusion is a spherical cap but membrane is taken out of the cell with membrane exchange between the cell and the protrusion.

Case 1 is equivalent to the one studied before, since the protrusion and the cell are independent. The spreading curve starts linearly and it saturates at longer time. The slope of the spreading curve sets a characteristic time proportional to the size of the protrusion (see Eq. (47)). This conclusion applies if the size of the protrusion is large enough with respect to the other lengths defined in the problems. The time at which the spreading curve attains 2/3 of the limit sets another characteristic time. When the cell and the protrusion cannot exchange membrane, this characteristic time is equivalent to the one defined by the slope at short time. From now on, we concentrate on case 2.

Scaling shows that if membrane exchange between the protrusion and the cell takes place, the scale at which the surface tension increases during spreading differs by a factor  $R_2^2(\theta)/R_1^2$  from the uniform spreading case. This scaling factor comes from the definition of the surface tension

$$d\sigma = C \frac{dA}{\mathcal{A}_T} \quad (55)$$

where  $\mathcal{A}_T$  is set by the cell of radius  $R_1(\theta_1)$  which serves as a reservoir. This factor does not play a role at the early stages of spreading. Thus, we conclude :

1. The slope at short time is still inversely proportional to the size of the protrusion  $R_2(0)$  (see Eq. (47)).
2. The time at which the contact area is 2/3 of the saturation limit depends, however, on geometry. We find that the surface tension increases with  $\theta_2$  as

$$\Delta\sigma \propto C \frac{R_2(0)^2}{R_1(\theta_1)^2} \theta_2^3 \quad (56)$$

so that small protrusions have large contact angles. Assuming that  $\alpha^3 t_s^3 R_2(0)^2 / R_1(0)^2 = \text{const}$  gives the characteristic time at which saturation occurs, we find that  $t_s \propto R_2(0)^{1/3}$  instead of  $t_s \propto R(0)$  in the uniform case.

To conclude this section, we note that a stress builds up on the two sides of the protrusion when the contact area increases (see Appendix E). In turn, this quadratic increase of energy can be used as a mechanical signal to start a new protrusion on the sides of the existing protrusion, as suggested by experiments [29, 30].

### Conclusion and outlook

The purpose of this paper is to point out that the characteristic spreading curve of the contact area can be analyzed within a simple physical model which contains the regulation of the actin polymerisation rate. The model assumes that this rate is controlled by the shear stress at the border of the contact area. The key parameter of the theory is the relative increase of tension during spreading. This parameter controls not only the rate of spreading but also the dependence of the spreading rate upon variations of the microscopic parameters. As a result the model can explain how the macroscopic observables change upon variations of these parameters, but it cannot explain the molecular basis of this regulation. The key point is to correlate how these parameters vary with the concentration of the molecular species at work in shape remodelling.

To conclude, we summarize some of the key elements of our work :

1. It should be interesting to measure the mechanical forces normal to the substrate. Our model predicts that bending is enough to get a non-trivial variation of the height variable with normal forces which change sign at the margin of the contact area.
2. The slope of the relative increase of contact area for each protrusion is linear at short time and it depends on the size of the protrusions before spreading. Only in the case of axisymmetric spreading, the characteristic time at which the spreading curve saturates is given by the characteristic time set by the initial slope. In all other cases, we expect geometrical factors and non-linear dependence as a function of the size of the protrusion.

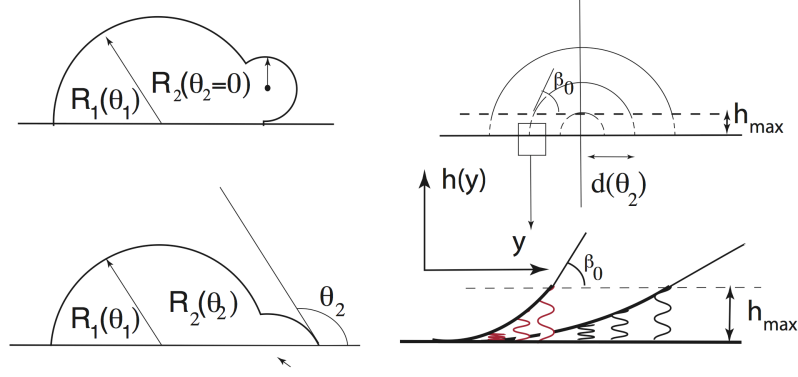


FIG. 9: Geometrical model for a pseudopod which is schematized as a spherical protrusion protruding out a cell. The two figures on the left represent the side views of a protrusion spreading on the substrate. The top figure on the right column is the top view of the contact lines when the size of the cell is much larger than the characteristic size of the protrusion, so the cell corresponds to the  $h = 0$  line in the  $(y, h)$  plane of the substrate. During spreading, its center moves downward and  $R_2(\theta_2)$  increases (see Appendix D). Viewed from the top, the contact line is half of a circle which intersects the line  $h(y) = 0$  at right angle when the center moves along a straight line perpendicular to the substrate. The characteristic height  $h_{max}$  is defined in Appendix E using a peeling geometry. It is of the order of a few 10 of n.m. During spreading,  $d(\theta_2)$  increases linearly with  $\theta_2$  and so  $\beta_0$ . The inset is a cartoon which represents the elastic foundation which mimics the membrane-cytoskeleton attachment near the points where the protrusion intersects the cell and it describes the peeling of this elastic foundation with increasing the contact area.

3. The slope of the spreading curve depends on the membrane cytoskeleton adherence which, in turn, depends on a number of lipid species and on some motor proteins. Among the lipids involved in the attachment of the membrane to the cytoskeleton, phosphoinositide lipids such as  $\text{Pip}_2$  play a central role in the signalling pathway[66]. The increase in  $\text{Pip}_2$  strengthens the adhesion between the two components. Moreover, the production of  $\text{Pip}_3$  from  $\text{Pip}_2$  favors actin polymerisation[14, 26]. Thus a concomitant decrease in  $\text{Pip}_2$  with an increase in  $\text{Pip}_3$  decreases  $C$  but increases  $k_{on}$ , two of the parameters which are taken into account in the model. The adherence of the membrane to the cytoskeleton may also be altered by using mutant cells. Knocking out motor proteins ezrin, myosin I or using talin-defective cells may be therefore appropriate to test how the rate of spreading depends on these proteins.
4. When spreading stops, the contact area between the cell and the substrate depends on the relative increase of surface tension for the effective membrane which is not in adhesion with the underlying cortex. Decreasing the surface tension before spreading should increase the contact area after spreading and increase the rate of spreading at constant polymerization rate. This result is consistent with Ref. [50] where a detergent was used to change the membrane tension. We note, however, that the surface tension must be sufficiently large enough to have a well defined mechanical stress in the adhesive belt in order to stimulate actin polymerization.
5. Our model points out the role of the mechanical stress localized at the margin of the contact area. This stress is not uniformly distributed around the contact line with the substrate. The protrusion of Fig. 9 shows, for example, that it is localized on the two sides corners of the pseudopod and that it increases with spreading. Under the hypothesis that biochemistry is stress dependent, this indicates that the next spreading event may be localized in the vicinity of the two sides of an existing pseudopod. This remark seems to be confirmed by the analysis of experimental data[30], but it has to be confirmed by analyzing the exact molecular links with actin polymerisation.

### Acknowledgments

B.F. thanks Prof. M. Block, Dr. C. Albigez-Rizo, Dr. E. Planus and Dr. O. Destaing for very useful comments and discussions.

### APPENDIX A: EFFECTIVE POLYMERIZATION RATE

We define in this appendix an effective polymerization rate  $k_{on}^0$ . We show that the matching conditions at the frontier  $A$  of the adhesive belt allow to compute  $V_{\parallel}$  as a function of  $k_{on}^0$  and that this condition is equivalent to define  $V_{\perp}(\psi)$  proportional to the curvature ( $1/R = d\psi/ds$ ) in the adhesive belt. We show that :

$$V_{\perp} = \frac{k_{on}^0}{\lambda_a^2 R} \quad (\text{A1})$$

Defining the actin polymerization rate in this way is useful, since it has been reported that curvature enhances the activity of key proteins involved in actin polymerization (see [25] for example). This appendix shows also that if  $V_{\perp}$  is defined this way, we can compute the speed  $V_{\parallel}(\theta)$  not only at point  $A$  but also in its vicinity without changing the value of  $V_{\parallel}$  since the product  $\psi R$  is constant along the arc in the vicinity of  $A$ .

Let us consider the rate of change of the line which simulates the deformations of the adhesive belt as a function of the angle  $\psi$  that makes the tangent with the  $x$ -axis. Because the rate of polymerization couples to the change of  $\psi$  per unit time, i.e.  $d\psi/dt$ , we define this rate as  $M(\psi)$  and we write

$$\frac{\partial\psi}{\partial t} = M(\psi) \quad (\text{A2})$$

The problem is to find a definition of  $M(\psi)$ . Since  $\psi$  is small in the adhesive belt, we can expand  $M(\psi)$  to lowest order in  $\psi$  to get the changes of  $\psi$  with time in a coordinate system fixed with respect to the substrate

$$\frac{\partial\psi}{\partial t} = -k_{on}^0\psi \quad (\text{A3})$$

where  $k_{on}^0$  is an effective polymerisation rate in units of  $\text{sec}^{-1}$ . The minus sign gives that the angle  $\psi$  that makes the tangent with the substrate decreases when the cell spreads.

In principle,  $k_{on}^0$  should be determined from a more microscopic model to include the effect of the branched polymerization of actin in the adhesive belt (i.e. the dentritic nucleation model) . In this work,  $k_{on}^0$  is a constant for fixed macroscopic contact angle  $\theta$ . The product  $k_{on}^0\psi$  simulates the enhancement of actin polymerization in the adhesive belt at the margin of the contact area where  $\psi$  increases.

To get a second equation for the variations of  $\psi$ , we write that the rate of variations of  $\psi$  is the first derivative of the velocity normal to the line  $z(x)$ . This exact formula can be simplified for small angle  $\psi$ , and we have using Eq. (3)

$$\frac{\partial\psi}{\partial t} = -\frac{dV_{\perp}}{dx} \approx V_{\parallel} \frac{d\psi}{dx} \quad (\text{A4})$$

where  $d\psi/dx$  is the inverse of the radius of curvature at point  $A$ . Let  $R_A$  be this radius. Since for small  $\theta$ ,  $V_{\parallel}$  is a characteristic polymerisation rate independent of the macroscopic angle  $\theta$ , Eqs (A3) and (A4) are consistent if the product  $R_A\psi(x=0)$  is independent of  $\theta$ .

We can now use Eqs. (35) and (36) which result from solution of the shape problem. We find

$$R(\theta)\psi(\theta) = \frac{1}{\lambda_a} \quad (\text{A5})$$

which independent of the macroscopic angle  $\theta$ . Thus, the speed  $V_{\parallel}$  is proportional to the effective polymerization rate  $k_{on}^0$

$$V_{\parallel} = \frac{1}{\lambda_a} k_{on}^0 \quad (\text{A6})$$

where the length  $1/\lambda_a$  is the characteristic length of the adhesive belt. Using  $V_{\perp} = V_{\parallel}\psi$  gives Eq. (A1).

In conclusion, the hypothesis of a constant speed of translation (Cf. Eq. (A4) plus the constraint of mechanical equilibrium (Cf. Eq. (A5) ) give a speed  $V_{\perp}$  proportional to the curvature.

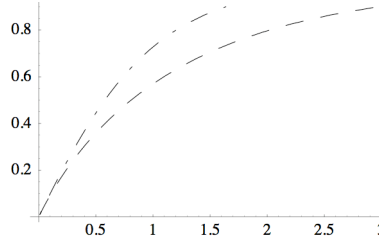


FIG. 10: Plot of the function  $w(t)$  defined in Eq. (B3) for two values of the parameter  $\eta$  (dot-dashed line,  $\eta = 0.01$ , dashed line,  $\eta = 0.9$ ). Both curve have the same tangent at the origin.

## APPENDIX B: EFFECT OF VISCOUS DRAG

We study in this appendix the effect of the viscous term  $\eta$  defined in Eq. (6) on the shape of the spreading curve. This term is conventionally used in viscoelastic theory to simulate membrane flow. To make notations simple, we renormalize  $\eta$  so that it is dimensionless. When  $\eta$  is non-zero the kinetics of the spreading curve for a sphere is described by an equation similar to Eq. (46)

$$\frac{d^2w}{dt^2} = -\alpha \left( \frac{dw^2}{dt} + \frac{\eta}{\alpha} \frac{d^2w^2}{dt^2} \right) \quad (\text{B1})$$

with the intermediate variable

$$w = \frac{\theta^2}{\theta_m^2} \quad (\text{B2})$$

proportional to the contact area when  $\theta_m$  is small. The solution of this equation is

$$\text{ArgTanh}(w) - \eta \ln(1 - w^2) = \alpha t \quad (\text{B3})$$

so that  $w \propto \alpha t$  when  $t$  goes to zero. Thus adding a visco-elastic component leaves the slope of the spreading curve unchanged near the origin, but the characteristic time at which it saturates is larger.

## APPENDIX C: EULER EQUATION

Eq. (17) is the potential we want to minimize. It differs from the usual bending potential for membranes[24] because of the surface tension which is usually taken as a Lagrange's multiplier for the constraint of total area. In our case,  $\sigma$  is a tensile stress in the direction  $\mathbf{u}_\theta$ . To minimize Eq. (17) with respect to  $\psi(s)$  (or  $\phi(s)$  since  $\psi(s) + \phi(s) = \theta$ ) we choose  $\psi(s)$  and  $x(s)$  as independent variables. Therefore, we introduce a Lagange's multiplier[44]  $\lambda_x(s)$  with a potential  $L$

$$L(\psi, \dot{\psi}, x, \dot{x}, \lambda_x) = \int ds \mathcal{L} = F + \int ds \lambda_x(s) \left( \frac{dx}{ds} - \cos \psi \right) \quad (\text{C1})$$

Independent variations with respect to  $x \rightarrow x + \delta x$ ,  $\psi \rightarrow \psi + \delta \psi$  and  $\lambda_x \rightarrow \lambda_x + \delta \lambda_x$  lead to

$$\begin{aligned} L = & \int_{s_A}^{s_B} ds \left[ \frac{\partial \mathcal{L}}{\partial \psi} - \frac{d}{ds} \left[ \frac{\partial \mathcal{L}}{\partial \dot{\psi}} \right] \right] + \int_{s_A}^{s_B} ds \left[ \frac{\partial \mathcal{L}}{\partial x} - \frac{d}{ds} \left[ \frac{\partial \mathcal{L}}{\partial \dot{x}} \right] \right] \\ & + \int_{s_A}^{s_B} ds \left[ \frac{\partial \mathcal{L}}{\partial \lambda_x} - \frac{d}{ds} \left[ \frac{\partial \mathcal{L}}{\partial \dot{\lambda}_x} \right] \right] = 0 \end{aligned} \quad (\text{C2})$$

with the boundary conditions

$$\left[ \frac{\partial \mathcal{L}}{\partial \dot{x}} \delta x(s) \right]_{s_A}^{s_B} + \left[ \frac{\partial \mathcal{L}}{\partial \dot{\psi}} \delta \psi(s) \right]_{s_A}^{s_B} + \left[ \frac{\partial \mathcal{L}}{\partial \dot{\lambda}_x(s)} \delta \lambda_x(s) \right]_{s_A}^{s_B} + \mathcal{L}(s_B) \delta s_B - \mathcal{L}(s_A) \delta s_A = 0 \quad (\text{C3})$$

From (C2), we get :

$$\begin{aligned}\kappa_m \frac{d^2\psi}{ds^2} + \sigma \sin(\theta - \psi) - \lambda_x(s) \sin \psi &= 0 \\ \frac{dx}{ds} &= \cos \psi \\ \frac{d\lambda_x}{ds} &= 0\end{aligned}\tag{C4}$$

The last equation gives  $\lambda_x(s) = \text{const.}$  To recover Eq. (17), we now show that  $\lambda_x = 0$ .

By analogy with a mechanical problem, we define a conserved Hamiltonian  $\mathcal{H}$ , since  $L$  does not depend explicitly on  $s$  (with  $s$  playing the role of the time)

$$\mathcal{H} = \mathcal{L} - \dot{\psi} \frac{\partial \mathcal{L}}{\partial \dot{\psi}} - \dot{x} \frac{\partial \mathcal{L}}{\partial \dot{x}} - \dot{\lambda}_x(s) \frac{\partial \mathcal{L}}{\partial \dot{\lambda}_x(s)}\tag{C5}$$

Now we use the boundary condition at  $A$  and  $B$ . Since the angles  $\psi(s_A)$  and  $\psi(s_B)$  are fixed, we have

$$\begin{aligned}(\psi + \delta\psi)(s_A + \delta s_A) = \psi(s_A) &\Rightarrow \delta\psi(s_A) = -\dot{\psi}(s_A) \delta s_A \\ (\psi + \delta\psi)(s_B + \delta s_B) = \psi(s_B) &\Rightarrow \delta\psi(s_B) = -\dot{\psi}(s_B) \delta s_B\end{aligned}\tag{C6}$$

with similar equations for  $\delta x_A$  and  $\delta x_B$ . Using now Eq. (C3), we get

$$\left[ \frac{\partial \mathcal{L}}{\partial \dot{x}} (\delta x(s) - \dot{x} \delta s) \right]_{s_A}^{s_B} + \mathcal{H}(\delta s_A - \delta s_B) = 0\tag{C7}$$

We now compare different paths with fixed length between  $A$  and  $B$ ,  $s_B = s_A + \text{const.}$  Thus  $\delta s_A = \delta s_B$ . Since

$$\frac{\partial \mathcal{L}}{\partial \dot{x}} = \lambda_x$$

and, since  $\delta x_B$  is arbitrary we show that  $\lambda_x$  is zero.

#### APPENDIX D: GEOMETRICAL MODEL FOR THE PROTRUSION

Let us consider the family of spheres of radius  $R_2(\theta_2)$  whose centers are positioned on a straight line perpendicular to the substrate. We define the volume  $V(\theta_2)$  as the part of the sphere of radius  $R_2(\theta_2)$  lying above the substrate and outside the sphere of radius  $R_1(\theta_1)$ . As before,  $R_1(\theta_1)$  simulates the cell. When  $R_1(\theta_1) \gg R_2(\theta_2)$  the two volumes intersect each other along a circular arc. This defines an area  $A_{1,2}$  (grey part in Fig. 9) with

$$A_{1,2} = (\pi - \theta_2) R_2^2(\theta_2) + \frac{1}{2} R_2^2(\theta_2) \sin(2\theta_2)\tag{D1}$$

with a distance  $2d(\theta_2)$  between the two points defined by the intersection of this circular arc and the substrate

$$d(\theta_2) = R_2(\theta_2) \sin(\theta_2)\tag{D2}$$

Finally, the constraint of equal volume  $V(\theta_2)$  independent of  $\theta_2$  fixes the relationship between  $R_2(\theta_2)$  and  $\theta_2$ .

We choose arbitrarily one member of this family  $\theta_2^0$  as the protrusion before it spreads. Thus,  $\theta_2^0$ ,  $R_2(\theta_2^0)$  and  $d(\theta_2^0)$  are fixed by the local softening of the cytoskeleton.

What happens next is geometrically equivalent to what has been described for uniform spreading. The center of the sphere moves downward and its radius  $R_2(\theta_2)$  increases to keep the volume constant. To keep a minimal set of parameters, we will assume that the center of the sphere of radius  $R_2(\theta_2)$  moves along the line perpendicular to the substrate. Viewed from below, the area of contact is defined by a family of concentric half circles with radius  $d(\theta_2)$ .

Keeping the spherical variational calculation, we can compute the surface tension from

$$d\sigma = C \frac{dA}{A}\tag{D3}$$

Since the cell is much larger than the protrusion,  $\mathcal{A}$  in the denominator is constant. The integration is now straightforward and one finds

$$\sigma = \sigma_0 + C (\mathcal{A}_d(\theta_2) + \mathcal{A}_c(\theta_2)) \quad (\text{D4})$$

where the area of the dorsal part is

$$\mathcal{A}_d(\theta_2) = \pi R_2^2(\theta_2)(1 + \cos \theta_2) - \mathcal{A}_{1,2}(\theta_2) \quad (\text{D5})$$

and the contact area

$$\mathcal{A}_{1,2}(\theta_2) = \pi R_2^2(\theta_2) \sin^2 \theta_2 \quad (\text{D6})$$

Note that the area  $\mathcal{A}_{1,2}(\theta_2)$  must be subtracted from the gain area taken from the cell. Finally, Taylor expanding Eq. (D4), one finds that  $\sigma$  increases as  $\theta_2^3$  because of the  $\mathcal{A}_{1,2}(\theta_2)$  term.

## APPENDIX E: PEELING MODEL FOR THE PROTRUSIONS

The calculation for the protrusion being variational, the force balance equation between the protrusion and the cell is not satisfied. If we concentrate on the contact plane between the cell and the substrate, we see from Eq. (D2) that  $d(\theta_2)$  increases linearly with  $\theta_2$ . This indicates that the junction between the protrusion and the cell is stressed during spreading. We model this elastic contact using a peeling mechanism for the membrane attached to the cytoskeleton.

To model this stress we concentrate on a 2-d geometry. We describe the contact region protrusion - cell - substrate by an elastic foundation of modulus  $k_l$ , where  $k_l$  is the rigidity of a linker molecule. Assuming weak cohesion forces, the number of bound linkers is given by

$$n_l(h) = \frac{n_0}{1 + \exp [B - \frac{1}{2}k_l(h - h_0)^2/k_B T]} \quad (\text{E1})$$

where  $k_l(h - h_{max})$  is the strain.  $B \approx 20 k_B T$  is the activation energy of an unstressed bond. This defines a maximum displacement  $h_{max}$  above which the linker is broken ( $h_{max} = 2h_0 = 2(2B/k_l)^{1/2} \approx 20 - 200\text{n.m.}$ [65]).

Returning to the protrusion model, we can model the contact line on the substrate as an arc of circle if  $h(y) > h_{max}$  and as an elastic foundation for  $h(y) < h_{max}$ . The calculation is similar to the one made for the adhesive belt and the shape of the elastic foundation is a damped exponential ( $\lambda_l \propto (n_0 k_l / \kappa_a)^{1/4}$ ).

$$h(y) = \exp [-\lambda_l y] \{h_{max} \cos(\lambda_l y) + C \sin(\lambda_l y)\} \quad (\text{E2})$$

where for  $y < 0$ ,  $h(y) < h_{max}$ . For the shape (E2) to match the arc of circle at angle  $\beta_0$ , we have

$$C = \lambda_l^{-1} (\beta_0 + \lambda_l h_{max}) \quad (\text{E3})$$

Since

$$\cos(\beta_0) = \frac{h_{max}}{d(\theta_2)} \quad (\text{E4})$$

increasing the area of contact, increases  $\theta_2$  which, in turn, increases  $d(\theta_2)$  (Cf. Eq. (D2)) : Thus, by Eq. (E4),  $\beta_0$  increases and the elastic foundation is more and more stressed with an asymptotic value reached for  $d(\theta_2) \approx 10h_{max}$ .

In conclusion, stress builds up at the junction between the cell and the protrusion during spreading. Breaking the bonds releases the elastic energy stored in the junction and equilibrium can be maintained as  $\theta_2$  increases. This places an upper bound on the angle  $\beta_0$  above which the membrane is detached from the cytoskeleton. To compute this threshold, let  $G(\beta)$  be the energy stored in the junction. We find :

$$G(\beta_0) = \kappa \lambda_l \left[ \lambda_l^2 h_{max}^2 + (\beta_0 + \lambda_l h_{max})^2 \right] \quad (\text{E5})$$

Let  $dG/d[d(\theta_2)]$  be the rate of increase of energy in the junction when  $d(\theta_2)$  increases by  $d[d(\theta_2)]$  and let  $w$  be the adhesion energy between the membrane and the cytoskeleton. We compute the maximum angle in the junction from the condition

$$dG/d[d(\theta_2)] = w \quad (\text{E6})$$

or  $\beta_0 \approx w/(2\kappa)$  if  $\lambda_1 h_{max} \approx 1$ . For  $\beta_0$  larger than this value, the membrane will spontaneously detach from the cytoskeleton.

- 
- [1] C. Aguado-Velasco and M. Bretscher. Circulation of plasma membrane in dictyostelium. *Mol. Bio. Cell*, 10:4419–4427, 1999.
- [2] A. R. Bausch, F. Ziemann, A. A. Boulbitch, K. Jacobson, and E. Sackmann. Local measurements of viscoelastic parameters of adherent cell surfaces by magnetic bead microrheometry. *Biophys J*, 75(0006-3495 (Print)):2038–49, 1998.
- [3] A. Boulbitch, R. Simson, D. Simson, R. Merkel, W. Häckl, M. Bärmann, and E. Sackmann. Shape instability of a biomembrane driven by a local softening of the underlying actin cortex. *Phys Rev E Stat Phys Plasmas Fluids Relat Interdiscip Topics*, 62(3 Pt B):3974–3985, Sep 2000.
- [4] D. Bray. *Cell Movements : From Molecules to Motility*. Garland Publishing, New York, 2nd edition, 2001.
- [5] M. C. Brown and C. E. Turner. Paxillin: adapting to change. *Physiol Rev*, 84(4):1315–1339, 2004.
- [6] F. Chamaraux, S. Fache, F. Bruckert, and B. Fourcade. Kinetics of cell spreading. *Phys Rev Lett*, 94(15):158102–158102, Apr 2005.
- [7] G. T. Charras, C.-K. Hu, M. Coughlin, and T. J. Mitchison. Reassembly of contractile actin cortex in cell blebs. *J Cell Biol*, 175(3):477–490, 2006.
- [8] O. Collin, P. Tracqui, A. Stephanou, Y. Usson, J. Clement-Lacroix, and E. Planus. Spatiotemporal dynamics of actin-rich adhesion microdomains: influence of substrate flexibility. *J Cell Sci*, 119(Pt 9):1914–1925, 2006.
- [9] C. C. Cunningham. Actin polymerization and intracellular solvent flow in cell surface blebbing. *J Cell Biol*, 129(6):1589–1599, 1995.
- [10] D. Cuvelier, O. Rossier, P. Bassereau, and P. Nassoy. Micropatterned "adherent/repellent" glass surfaces for studying the spreading kinetics of individual red blood cells onto protein-decorated substrates. *Eur Biophys J*, 32(0175-7571 (Print)):342–54, 2003.
- [11] D. Cuvelier, M. Thery, Y.-S. Chu, S. Dufour, J.-P. Thiery, M. Bornens, P. Nassoy, and L. Mahadevan. The universal dynamics of cell spreading. *Curr Biol*, 17(8):694–699, 2007.
- [12] D. E. Discher, P. Janmey, and Y.-L. Wang. Tissue cells feel and respond to the stiffness of their substrate. *Science*, 310(1095-9203 (Electronic)):1139–43, 2005.
- [13] H. Döberheiner, B. Dublin-Thaler, G. Giannone, H. Xenias, and M. Sheetz. Dynamic phase transition in cell spreading. *Phys. Rev. Lett.*, 93(108105(4)), 2004.
- [14] D. Dormann, G. Weijer, S. Dowler, and C. Weijer. In vivo analysis of 3-phosphoinositide dynamics during Dictyostelium phagocytosis and chemotaxis. *J Cell Sci*, 117(Pt 26):6497–6509, Dec 2004.
- [15] O. du Roure, A. Saez, A. Buguin, R. Austin, P. Chavrier, P. Siberzan, and B. Ladoux. Force mapping in epithelial cell migration. *Proc Natl Acad Sci U S A*, 102(7):2390–2395, Feb 2005.
- [16] S. Fache, J. Dalous, M. Englund, C. Hansen, F. Chamaraux, B. Fourcade, M. Satre, P. Devreotes, and F. Bruckert. Calcium mobilization stimulates dictyostelium discoideum shear-flow-induced cell motility. *J Cell Sci*, 118(0021-9533):3445–57, 2005.
- [17] D. Garrivier, E. Decavé, Y. Brechet, F. Bruckert, and B. Fourcade. Peeling model for cell detachment. *Eur. Phys. J. E*, 8:79–97, 2002.
- [18] G. Giannone, B. J. Dubin-Thaler, H.-G. Dobereiner, N. Kieffer, A. R. Bresnick, and M. P. Sheetz. Periodic lamellipodial contractions correlate with rearward actin waves. *Cell*, 116(0092-8674 (Print)):431–43, 2004.
- [19] G. Giannone, G. Jiang, D. H. Sutton, D. R. Critchley, and M. P. Sheetz. Talin1 is critical for force-dependent reinforcement of initial integrin-cytoskeleton bonds but not tyrosine kinase activation. *J Cell Biol*, 163(2):409–419, 2003.
- [20] G. Giannone, P. Rondé, M. Gaire, J. Beaudouin, J. Haiech, J. Ellenberg, and K. Takeda. Calcium rises locally trigger focal adhesion disassembly and enhance residency of focal adhesion kinase at focal adhesions. *J Biol Chem*, 279(27):28715–28723, Jul 2004.
- [21] N. S. Gov and A. Gopinathan. Dynamics of membranes driven by actin polymerization. *Biophys J*, 90(2):454–69, 2006.
- [22] O. Hamill and B. Martinac. Molecular basis of mechanotransduction in living cells. *Physiological Review*, 81(2):686–728, 2001.
- [23] A. Hategan, K. Sengupta, S. Kahn, E. Sackmann, and D. Discher. Topographical pattern dynamics in passive adhesion of cell membranes. *Biophys J*, 87(5):3547–3560, Nov 2004.
- [24] W. Helfrich and R. M. Servuss. Undulations, steric interaction and cohesion of fluid. membranes. *Nuovo Cimento*, 3D:137–151, 1984.
- [25] S. Hübner, A. D. Couvillon, J. A. Käs, V. A. Bankaitis, R. Vegners, C. L. Carpentier, and P. A. Janmey. Enhancement of phosphoinositide 3-kinase (pi 3-kinase) activity by membrane curvature and inositol-phospholipid-binding peptides. *Eur. J. Biochem.*, 258(2):846–853, 1998.
- [26] R. Insall and O. Weiner. PIP3, PIP2, and cell movement—similar messages, different meanings? *Dev Cell*, 1(6):743–747, Dec 2001.
- [27] P. A. Janmey. Phosphoinositides and calcium as regulators of cellular actin assembly and disassembly. *Annu Rev Physiol*, 56(0066-4278 (Print)):169–91, 1994.
- [28] J.-F. Joanny, F. Julicher, and J. Prost. Motion of an adhesive gel in a swelling gradient: a mechanism for cell locomotion. *Phys Rev Lett*, 90(0031-9007 (Print)):168102, 2003.

- [29] S. Keller. *Étalement de Dictyostelium discoideum et rôle des protéines Phg2, PKD2 et TPC dans la motilité*. PhD thesis, Université Joseph Fourier - Grenoble - France, 2007.
- [30] S. Keller, S. Fache, F. Chamaraux, B. Fourcade, and F. Bruckert. Dictyostelium discoideum spreading on solid substrate: morphology and kinetics. *submitted to Biophysocal j.*, 2007.
- [31] L. Landau and E. Lifshitz. *Theory of elasticity*. Pergamon, 1970.
- [32] S. Linder and P. Kopp. Podosomes at a glance. *J Cell Sci*, 118(Pt 10):2079–2082, 2005.
- [33] C. Manahan, P. Iglesias, Y. Long, and P. Devreotes. Chemoattractant signaling in dictyostelium discoideum. *Annu Rev Cell Dev Biol*, 20:223–253, 2004.
- [34] V. Martel, C. Racaud-Sultan, S. Dupe, C. Marie, F. Paulhe, A. Galmiche, M. R. Block, and C. Albiges-Rizo. Conformation, localization, and integrin binding of talin depend on its interaction with phosphoinositides. *J Biol Chem*, 276(24):21217–21227, 2001.
- [35] D. Maugis. *Contact, Adhesion and Rupture of Elastic Solids*. Springer, 2000.
- [36] A. Mogilner. On the edge: modeling protrusion. *Curr Opin Cell Biol*, 18(0955-0674 (Print)):32–9, 2006.
- [37] A. Mogilner and L. Edelstein-Keshet. Regulation of actin dynamics in rapidly moving cells: A quantitative analysis. *Bio. Phys. J.*, 83:1237–1258, 2002.
- [38] A. Mogilner and G. Oster. Cell motility driven by actin polymerization. *Biophys J*, 71(0006-3495 (Print)):3030–45, 1996.
- [39] A. Mogilner and B. Rubinstein. The physics of filopodial protrusion. *Biophys J*, 89(0006-3495 (Print)):782–95, 2005.
- [40] S. Munevar, Y. Wang, and M. Dembo. Regulation of mechanical interactions between fibroblast and substratum by stretch-activated ca<sup>2+</sup> entry. *J. Cell Science*, 117:85–92, 2004.
- [41] T. Nebl and P. Fisher. Intracellular ca<sup>2+</sup> signals in dictyostelium chemotaxis are mediated exclusively by ca<sup>2+</sup> influx. *J. Cell Sci.*, 110:2845–2853, 1997.
- [42] D. Pantaloni, C. L. Clainche, and M.-F. Carlier. Mechanism of actin-based motility. *Science*, 292:1502–1506, 2001.
- [43] P. Pelcé. *New visions on Form and Growth*. Oxford University Press, 2004.
- [44] M. Peterson. An instability of the red blood cell shape. *J. Appl. Phys.*, 57(5):1739–1742, 1985.
- [45] A. Pierres, A. Benliel, D. Touchard, and P. Bongrand. How cells tiptoe on adhesive surfaces before sticking. *Biophys J*, page in press, 2008.
- [46] A. Pierres, P. Eymeric, E. Baloche, D. Touchard, A.-M. Benliel, and P. Bongrand. Cell membrane alignment along adhesive surface : Contribution of active and passive cell processes. *Biophys. J.*, 84:2058–2070, 2003.
- [47] T. D. Pollard, L. Blanchoin, and R. D. Mullins. Molecular mechanisms controlling actin filament dynamics in nonmuscle cells. *Annu Rev Biophys Biomol Struct*, 29(1056-8700 (Print)):545–76, 2000.
- [48] T. D. Pollard and G. Borisy. Cellular motility driven by assembly and disassembly of actin filaments. *Cell*, 112:453–465, 2003.
- [49] J. Prost. *Physics of bio-molecules and cells*, volume LXXV, chapter The physics of listeria propulsion, pages 217–236. EDP-Sciences and Springer -Verlag, Les Ulis, 2002.
- [50] D. Raucher and M. Sheetz. Cell spreading and lamellipodial extension rate is regulated by membrane tension. *J. Cell. Bio.*, 148:127–136, 2000.
- [51] D. Raucher and M. P. Sheetz. Cell spreading and lamellipodial extension rate is regulated by membrane tension. *J Cell Biol*, 148(0021-9525 (Print)):127–36, 2000.
- [52] A. Ridley, M. Schwartz, K. Burridge, R. Firtel, M. Ginsberg, G. Borisy, J. Parsons, and A. Horwitz. Cell migration: Integrating signals from front to back. *Science*, pages 1704–1709, 2003.
- [53] D. Riveline, E. Zamir, N. Q. Balaban, U. S. Schwarz, T. Ishizaki, S. Narumiya, Z. Kam, B. Geiger, and A. D. Bershadsky. Focal contacts as mechanosensors: externally applied local mechanical force induces growth of focal contacts by an mdia1-dependent and rock-independent mechanism. *J Cell Biol*, 153(0021-9525 (Print)):1175–86, 2001.
- [54] E. Sackmann, A. Bausch, and L. Vonna. *Physics of bio-molecules and cells*, volume LXXV, chapter Physics of Composite Cell Membranes, pages 239–309. EDP-Sciences and Springer -Verlag, Les Ulis, 2002.
- [55] M. P. Sheetz. Cell control by membrane-cytoskeleton adhesion. *Nat Rev Mol Cell Biol*, 2(1471-0072 (Print)):392–6, 2001.
- [56] R. Simson, E. Wallraff, J. Faix, J. Niewöhner, G. Gerisch, and E. Sackmann. Membrane bending modulus and adhesion energy of wild-type and mutant cells of dictyostellium lacking talin and cortexillins. *Biophys. J.*, 74:514–522, 1998.
- [57] J. V. Small, B. Geiger, I. Kaverina, and A. Bershadsky. How microtubules guide migrating cells ? *Nat Rev Mol Cell Biol*, 3:957–964, 2003.
- [58] M. Sokabe, F. Sachs, and Z. Jing. Quantitative video microscopy of patch clamped membranes stress, stress, capacitance, and stretch activation. *Biophys. J.*, 59:722–728, 1991.
- [59] J. Solon, J. Pecreaux, P. Girard, M.-C. Faure, J. Prost, and P. Bassereau. Negative tension induced by lipid uptake. *Phys Rev Lett*, 97(9):098103, 2006.
- [60] A. Stephanou, M. A. J. Chaplain, and P. Tracqui. A mathematical model for the dynamics of large membrane deformations of isolated fibroblasts. *Bull Math Biol*, 66(0092-8240 (Print)):1119–54, 2004.
- [61] M. Thery, A. Pepin, E. Dressaire, Y. Chen, and M. Bornens. Cell distribution of stress fibres in response to the geometry of the adhesive environment. *Cell Motil Cytoskeleton*, (0886-1544 (Print)), 2006.
- [62] M. Thery, V. Racine, A. Pepin, M. Piel, Y. Chen, J.-B. Sibarita, and M. Bornens. The extracellular matrix guides the orientation of the cell division axis. *Nat Cell Biol*, 7(1465-7392 (Print)):947–53, 2005.
- [63] V. Vogel and M. Sheetz. Local force and geometry sensing regulate cell functions. *Nat Rev Mol Cell Biol*, 7(4):265–275, 2006.
- [64] N. Wang, E. Ostuni, G. Whitesides, and D. Ingber. Micropatterning tractional forces in living cells. *Cell Motil Cytoskeleton*, 52(2):97–106, Jun 2002.

- [65] M. D. Ward, M. Dembo, and D. A. Hammer. Kinetics of cell detachment : Peeling of discrete receptor clusters. *Biophys. J.*, 67:2522–2534, 1994.
- [66] J. Xu, F. Wang, A. Van Keymeulen, P. Herzmark, A. Straight, K. Kelly, Y. Takuwa, N. Sugimoto, T. Mitchison, and H. R. Bourne. Divergent signals and cytoskeletal assemblies regulate self-organizing polarity in neutrophils. *Cell*, 114(0092-8674 (Print)):201–14, 2003.
- [67] K. Yoshida and T. Soldati. Dissection of amoeboid movement into two mechanically distinct modes. *J Cell Sci*, 119(Pt 18):3833–3844, 2006.
- [68] In this work, we coin the word protrusion as synonymous with pseudopod.
- [69] In this work elastic foundation is taken as synonymous with adhesive bridges